Precambrian Research 267 (2015) 311–322

Contents lists available at ScienceDirect

Precambrian Research

journal homepage: www.elsevier.com/locate/precamres

Paleoarchean sulfur cycling: Multiple sulfur isotope constraints from the Barberton Greenstone Belt, South Africa

Alice Montinaro[a,*], Harald Strauss[a], Paul R.D. Mason[b], Desiree Roerdink[b,c], Carsten Münker[d], Ulrich Schwarz-Schampera[e], Nicholas T. Arndt[f], James Farquhar[g], Nicolas J. Beukes[h], Jens Gutzmer[i], Marc Peters[a,l]

[a] Institut für Geologie und Paläontologie, Westfälische Wilhelms-Universität Münster, Münster, Germany
[b] Department of Earth Science, Utrecht University, Utrecht, The Netherlands
[c] Centre for Geobiology, University of Bergen, Bergen, Norway
[d] Institut für Geologie und Mineralogie, Universität zu Köln, Köln, Germany
[e] Bundesanstalt für Geowissenschaften und Rohstoffe, Hannover, Germany
[f] Université Joseph Fourier, St Martin d'Hères, France
[g] Department of Geology, University of Maryland, College Park, MD, USA
[h] Cimera, Geology Department, University of Johannesburg, Auckland Park, South Africa
[i] Institute für Mineralogie, Technische Universität Bergakademie Freiberg, Freiberg, Germany
[l] Center for Environmental Remediation, Institute for Geographic Science and Natural Resources Research, Chinese Academy of Science, Beijing 100101, China

ARTICLE INFO

Article history:
Received 25 June 2014
Received in revised form 1 June 2015
Accepted 23 June 2015
Available online 2 July 2015

Keywords:
Paleoarchean
Multiple sulfur isotopes
Barberton Greenstone Belt

ABSTRACT

Mass-dependent and mass-independent sulfur isotope fractionation archived in volcanic and sedimentary rocks from the Barberton Greenstone Belt (3550–3215 Ma), South Africa, provide constraints for sulfur cycling on the early Earth. Four different sample suites were studied: komatiites and tholeiites, barite, massive and disseminated sulfide ores, and non-mineralized black shales.

Variable but generally slightly positive $\delta^{34}S$ values between −0.7 and +5.2‰, negative $\Delta^{33}S$ values between −0.50 and −0.09‰, and a negative correlation between $\delta^{34}S$ and $\Delta^{33}S$ as well as between $\Delta^{33}S$ and $\Delta^{36}S$ for komatiites and tholeiites from the Komati Formation and from the Weltevreden Formation are outside the expected range of unfractionated juvenile sulfur. Instead, results suggest alteration of oceanic crustal rock sulfur through interactions with fluids that most likely derived their sulfur from seawater.

Barite from the Mapepe Formation displays positive $\delta^{34}S$ values between +3.1 and +8.1‰ and negative $\Delta^{33}S$ values between −0.77 and −0.34‰. The mass-independent sulfur isotope fractionation indicates an atmospheric sulfur source, notably photolytic sulfate, whereas the positive $\delta^{34}S$ values suggest bacterial sulfate reduction of the marine sulfate reservoir.

Non-mineralized black shale samples from the presumed stratigraphic equivalent of the Mapepe Formation show positive $\delta^{34}S$ values between 0.0 and +1.3‰ and positive $\Delta^{33}S$ values between +0.59 and +2.45‰. These results are interpreted to result from the reduction of photolytic elemental sulfur, carrying a positive $\Delta^{33}S$ signature.

Positive $\delta^{34}S$ values ranging from +0.7 to +3.5‰ and slightly negative $\Delta^{33}S$ values between −0.17 and −0.12‰ characterize massive and disseminated sulfides from the Bien Venue Prospect. Results suggest unfractionated juvenile magmatic sulfur source as the primary sulfur source, but a contribution from recycled seawater sulfate, which would be indicative of submarine hydrothermal activity, cannot be ruled out.

Massive and disseminated sulfides from the M'hlati prospect are distinctly different from massive and disseminated sulfide from the Bien Venue Prospect. They show negative $\delta^{34}S$ values between −1.2 and −0.1‰ and positive $\Delta^{33}S$ values between +2.66 and +3.17‰, thus, displaying a sizeable mass-independent

Abbreviations: GOE, Great oxidation event; BGB, Barberton Greenstone Belt.

* Corresponding author. Tel.: +49 251 8333972.
E-mail address: amont_01@uni-muenster.de (A. Montinaro).

http://dx.doi.org/10.1016/j.precamres.2015.06.008

sulfur isotopic fractionation. Again, these samples clearly exhibit the incorporation of an atmospheric MIF-S signal. The source of sulfur for these samples has positive $\Delta^{33}S$ values, suggesting a connection with photolytic elemental sulfur.
In conclusion, the sulfur isotope signatures in Paleoarchean rocks from the Barberton Greenstone Belt are diverse and indicate the incorporation of different sources of sulfur. For komatiites and tholeiites, barite and massive and possibly also disseminated sulfides from Bien Venue, multiple sulfur isotopes are related to ambient seawater sulfate and its photolytic origin, while massive and disseminated sulfides from M'hlati and non-mineralized black shales are related to a second (photolytic elemental sulfur) end member.

1. Introduction

The Archean Earth was considerably different from today: it was characterized by a predominance of oceanic over continental crust (Rollinson, 2007); the oceans were anoxic and characterized by ferruginous conditions (Holland, 2002; Canfield, 2004), possibly punctuated by occasional sulfidic intervals in the Neoarchean (Anbar et al., 2007; Garvin et al., 2009; Reinhard et al., 2009); the early atmosphere was reducing with abundant carbon dioxide and methane but essentially devoid of free atmospheric oxygen (Holland, 2006; but see Ohmoto et al., 2014 for a different view); life was entirely microbial in nature and is believed to have exclusively inhabited the marine realm (Holland and Turekian, 2004 and references therein).

The low atmospheric oxygen concentration is thought to have prevailed until early Paleoproterozoic time when the first significant rise in atmospheric oxygen abundance occurred around 2.4–2.3 Ga ago (Pufahl and Hiatt, 2012). This point in time is commonly referred to as the Great Oxidation Event (GOE), and it is thought to reflect a singular increase in atmospheric oxygen concentration above a level of 10^{-5} PAL (present atmospheric level; cf. Pavlov and Kasting, 2002). Contrasting studies, however, report the enrichment of redox sensitive metals as well as redox-related changes in their stable isotopic composition (such as Mo or Cr; e.g., Anbar et al., 2007; Frei et al., 2009; Crowe et al., 2013) suggesting an early onset of oxidative continental weathering, notably the presence of atmospheric oxygen some 50–100 or probably as early as 600 million years prior to the GOE.

Our present understanding about the anoxic nature of the Archean and early Paleoproterozoic atmosphere is generally based on the multiple sulfur isotope record. The discovery of mass-independently fractionated sulfur isotopes (MIF-S) by Farquhar et al. (2000; and subsequent reports, recently reviewed, e.g., by Johnston, 2011), expressed as distinctly positive and negative $\Delta^{33}S$ and $\Delta^{36}S$ signatures (>±0.3‰) and preserved in terrestrial rocks of Archean and early Proterozoic rocks older than 2.4 Ga, has become key evidence in our quest for reconstructing the temporal evolution of atmospheric oxygen.

This study investigates the multiple sulfur isotopic composition of different rock types that were derived from the 3.2 to 3.5 Ga old Barberton Greenstone Belt of South Africa and samples should collectively provide an understanding of Paleoarchean sulfur cycling. Specifically, we studied four different lithologies: (1) komatiites and tholeiites were selected as a potential archive of isotopically unfractionated juvenile sulfur pool ("mantle sulfur"); (2) barite is assumed to reflect the sulfur isotopic composition of ambient oceanic sulfate; (3) carbonaceous black shales without obvious signs of sulfide mineralization could reveal a biological signal; and (4) mineralized sulfidic black shales could have archived a hydrothermal signal. The prime scientific objective is to identify the principle sulfur sources and to characterize pertinent processes of inorganic and/or microbial sulfur cycling during Archean times.

2. Multiple sulfur isotope systematics and applications to the early Archean sulfur cycle

Multiple stable sulfur isotopes (^{32}S, ^{33}S, ^{34}S, ^{36}S) provide an unprecedented opportunity for identifying different sulfur sources and for reconstructing diverse (bio)geochemical processes that all characterize the pre-2.4 Ga sulfur cycle. Archived in sedimentary sulfide and sulfate minerals that formed in ancient Earth surface environments, mass-dependent and mass-independent sulfur isotopic fractionations may be utilized to deduce terrestrial as well as atmospheric processes. Conclusions based solely on the $\delta^{34}S$ record include (i) an unfractionated sulfur isotope signature in magmatic rocks (Clark and Fritz, 1997; Ono et al., 2003; Seal, 2006), (ii) slightly positive $\delta^{34}S$ values in hydrothermal precipitates reflecting a mixture between an unfractionated juvenile sulfur source and a contribution from recycled seawater sulfate (e.g., Peters et al., 2010), (iii) variable, yet generally positive $\delta^{34}S$ values in seawater precipitates, i.e. evaporitic sulfates and carbonate-associated sulfate (e.g., Kampschulte and Strauss, 2004), and (iv) highly variable, yet frequently negative $\delta^{34}S$ values in sedimentary sulfides attributed to biological sulfur cycling, notably bacterial sulfate reduction (e.g., Strauss, 1997; Canfield, 2001). Considering respective observations and underlying systematics of sulfur isotopic fractionation (reviewed, e.g., in Canfield and Raiswell, 1999; Johnston, 2011), the sedimentary records of Archean $\delta^{34}S_{sulfate}$ and $\delta^{34}S_{sulfide}$ have been regarded as generally reflecting (i) a low-sulfate ocean (Habicht et al., 2002; Crowe et al., 2014), whereas (ii) controversial views exist with respect to an early activity of biological sulfur cycling. Notably, the absence of consistently sizeable fractionations in ^{34}S has been regarded as evidence for a limited importance of biological sulfur cycling in Archean sedimentary surface environments (e.g., Strauss et al., 2003), despite individual reports of highly ^{34}S-depleted pyrite in Paleoarchean sedimentary rocks (e.g., Ohmoto et al., 1993; Shen et al., 2001, 2009; Philippot et al., 2007; Wu and Farquhar, 2013) and the notion from molecular biology that bacterial sulfate reduction represents an ancient metabolic pathway (Shen and Buick, 2004; Blumenberg et al., 2006; Philippot et al., 2007; Ueno et al., 2008; Shen et al., 2009; Johnston, 2011). Several recent reports of highly ^{34}S-depleted pyrite occurrences of early Archean age (e.g., Philippot et al., 2007; Ueno et al., 2008; Shen et al., 2009; Wacey et al., 2011a,b; Roerdink et al., 2013) strengthen the case for early biological sulfur cycling, even utilizing diverse metabolic pathways such as bacterial sulfate reduction, elemental sulfur reduction, elemental sulfur disproportionation, and sulfide oxidation.

The recognition that mass-independently fractionated sulfide and sulfate sulfur (MIF-S, i.e., non-zero $\Delta^{33}S$ and $\Delta^{36}S$ values) were present in a large number of Archean and early Proterozoic (>2.4 Ga) sedimentary rocks (e.g., Farquhar et al., 2000) provided an additional dimension in understanding sulfur isotope geochemistry.

MIF-S signatures are believed to result from the UV-induced photochemical dissociation of volcanogenic SO_2 (Farquhar, 2002). Its formation in and its transfer out of the atmosphere, and the subsequent preservation of this distinctive atmospheric signal in Earth surface sediments is possible only under essentially anoxic atmospheric conditions. Modeling results constrain the respective maximum level of atmospheric oxygen at 10^{-5} PAL (Pavlov and Kasting, 2002). The temporal evolution of the distinctive MIF-S signature exhibits substantial variability (for a recent review, see e.g., Johnston, 2011) during the Archean and early Paleoproterozoic. Termination of the MIF-S signature (i.e. in particular $\Delta^{33}S$ values >±0.3‰) is archived in 2.4–2.2 Ga old sedimentary rock successions in Canada (Papineau et al., 2007), South Africa (Guo et al., 2009) and on the Fennoscandian Shield (Reuschel et al., 2009).

Conceptual models for the pre-2.4 Ga sulfur cycling commence with an initial injection of volcanogenic sulfur dioxide into an anoxic atmosphere lacking an ozone shield. It is believed that this volcanogenic SO_2 (and by inference the pre-2.4 Ga mantle) carries no mass-independently fractionated sulfur. Consequently, oceanic crustal rocks are thought to have archived the unfractionated juvenile pre-2.4 Ga sulfur pool (Clark and Fritz, 1997; Ono et al., 2003; Seal, 2006; Ueno et al., 2008). This would mean that respective rocks should exhibit a zero per mil multiple sulfur isotope signature ($\delta^{34}S$, $\Delta^{33}S$, and $\Delta^{36}S = 0‰$). Support and confirmation of this initial assumption stems from MIF-S analyses of volcanic rocks (Farquhar et al., 2002; Ono et al., 2003; Ueno et al., 2008; Peters et al., 2010). Labidi et al. (2012) reported a $\delta^{34}S$ value of $-0.89 \pm 0.11‰$ for modern MORB at $\Delta^{33}S$ and $\Delta^{36}S$ values within error of the Canon Diablo Troilite reference.

Photochemical dissociation of this volcanogenic SO_2 has been suggested to result in the formation of a sulfate pool, carrying a negative $\Delta^{33}S$ signal and a pool of elemental sulfur, carrying a positive $\Delta^{33}S$ signal (e.g., Ono et al., 2003). The absence of free atmospheric oxygen prevents subsequent homogenization of these isotopically distinctly different photolytic sulfur pools. Following their transfer into Earth surface environments, both sulfur species enter the realm of terrestrial sulfur cycling with inorganic and/or microbially driven redox processes. These latter reactions are associated exclusively with mass-dependent sulfur isotopic fractionation, thereby preserving the initial atmospheric source signature (i.e. a negative or positive $\Delta^{33}S$ signature). As a consequence, sulfide and sulfate in pre-2.4 Ga sedimentary rocks exhibit distinctly different combinations of mass-dependently and mass-independently fractionated sulfur isotopes (for a recent review see, e.g., Johnston, 2011). Respective combinations (i.e. $\delta^{34}S$ versus $\Delta^{33}S$ and/or $\Delta^{33}S$ versus $\Delta^{36}S$) have been applied in order to differentiate sulfur sources (and mixtures thereof) and identify different (bio)geochemical processes.

Termed the "Archean array", a clear negative correlation of $\Delta^{33}S$ and $\Delta^{36}S$ values with a slope of −1 is utilized to uniquely identify the photolytic nature of sulfide and sulfate sulfur in sedimentary rocks of pre-2.4 Ga age (see Johnston, 2011).

Different combinations of $\delta^{34}S$ and (non-zero) $\Delta^{33}S$ values allow distinguishing the processing of respective photolytic sulfur in Earth surface environment as well as the mixing of different pools of photolytic and non-photolytic sulfur. The guiding principle in respective discussions has been the observation that a negative $\Delta^{33}S$ value would be indicative of photolytic sulfate as the ultimate sulfur source (with a positive $\delta^{34}S$ value as evident from the Archean barite deposits; e.g., Roerdink et al., 2012 and references therein) for sedimentary pyrite (exhibiting a negative $\Delta^{33}S$ value and negative and/or positive $\delta^{34}S$ values). It was further suggested that this combination of $\delta^{34}S$ and $\Delta^{33}S$ values could be indicative of microbial sulfate reduction under non-limiting (large fractionation in ^{34}S) or limiting (small fractionation in ^{34}S) oceanic sulfate abundance. In contrast, sedimentary pyrites exhibiting positive $\Delta^{33}S$ values and positive and/or negative $\delta^{34}S$ values were generally linked to the processing of photolytic elemental sulfur, either via sulfur reduction and/or disproportionation. Based on the statistical treatment of (then) available multiple sulfur isotope results from Paleoarchean sedimentary rocks Johnston (2011) defined two principal trajectories, with one starting from the origin and leading to the field of positive $\delta^{34}S$ and $\Delta^{33}S$ values (processing of elemental sulfur) and the other starting from the origin and leading to the field of negative $\delta^{34}S$ and $\Delta^{33}S$ values. Both trajectories exhibit a positive correlation between $\delta^{34}S$ and $\Delta^{33}S$.

In contrast, Philippot et al. (2007, 2012) reported a substantial number of multiple sulfur isotope results for pyrite from Paleoarchean sedimentary successions in Western Australia (Dresser Formation) and South Africa (Mapepe Formation) exhibiting a negative correlation between $\delta^{34}S$ and $\Delta^{33}S$ with a set of arrays going through the origin. These authors conclude that the entire range of multiple sulfur isotope values measured for Paleoarchean sulfides and sulfates, including strongly negative $\delta^{34}S$ and positive $\Delta^{33}S$ values (the felsic volcanic array of Philippot et al., 2012) can be satisfactorily explained by a mixing of sulfide sulfur derived from a photolytic elemental sulfur source and sulfide sulfur derived from sulfate reduction of photolytic oceanic sulfate. A specific MIF-S source reaction associated with pulses of felsic volcanism is advocated as the principal cause for observed extreme sulfur isotope signatures, but the involvement of different processes of microbially driven sulfur cycling is acknowledged.

Controversial discussions about the unique photochemical origin of mass-independently fractionated sulfur isotopes remain (Farquhar et al., 2010; Oduro et al., 2011), including propositions that mass-independent isotopic fractionation may also result from thermochemical sulfate reduction (Watanabe et al., 2009) or chemisorption reactions (Lasaga et al., 2008). However, this study will not address these views.

3. Geological setting

The 3550–3215 million years old Barberton Greenstone Belt (BGB) in South Africa represents one of the oldest well-preserved rock successions that has archived the environmental conditions that prevailed on the surface of our young planet. The BGB is located at the eastern edge of the Kaapvaal craton. The BGB is characterized by a sequence of volcanic and sedimentary rocks that includes oceanic and continental lithofacies. The Barberton Supergroup comprises three major lithostratigraphic units. These are, in ascending order, the Onverwacht Group (3550–3260 Ma), mainly composed of ultramafic to mafic volcanic rocks, the Fig Tree Group (3260–3225 Ma), consisting of greywacke, shale, chert and dacitic volcanic rocks, and the Moodies Group (3225–3215 Ma), composed of conglomerate, sandstone, siltstone and shale (Visser, 1956; Viljoen and Viljoen, 1969; Lowe and Byerly, 1999) (Fig. 1).

3.1. Komatiites and tholeiites

All but one komatiite and tholeiite samples stem from the Komati Formation, Onverwacht Group (3.5 Ga; Fig. 1). Five samples were collected from outcrop at the type locality on the eastern slope of Spinifex Creek. Samples Za-28a and Za 28b are classified as olivine-cumulate komatiites and samples Za-29a–c are classified as tholeiites (Münker et al., 2003, Patyniak, unpublished results).

These samples exhibit typical prehnite-pumpellyite to lower greenschist facies assemblages with pseudomorphs of serpentine after olivine and of amphibole and chlorite after pyroxene, some fresh pyroxene and olivine is still preserved. A detailed overview on the geology and petrology of the Spinifex Creek section is given in Dann (2000) and Robin-Popieul et al. (2012)

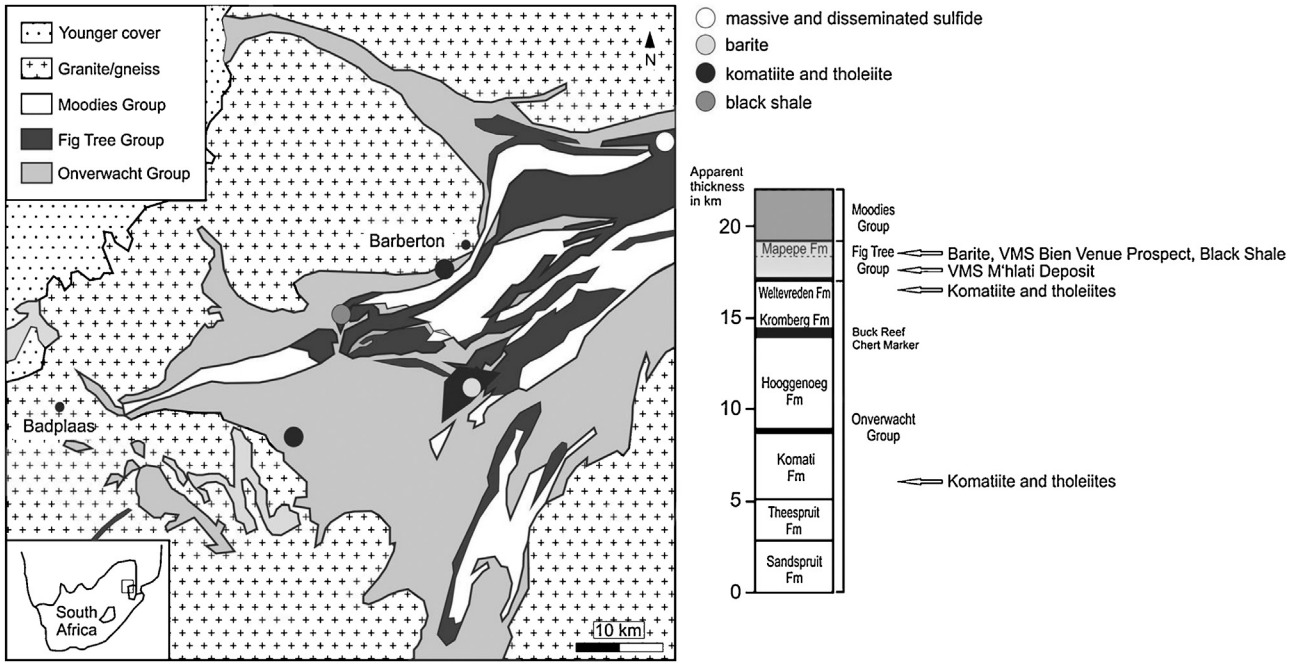

Fig. 1. Geological map of the Barberton Greenstone Belt (Roerdink et al., 2012, modified) with sample localities and stratigraphy of the BGB (Ward, 1999, modified) with apparent thicknesses of different units and approximate stratigraphic position of the samples studied here.

Ten further samples were obtained from drill core BARB1 that was drilled under the auspices of the International Continental Scientific Drilling Program (ICDP) project "Peering into the Cradle of Life" (http://www.peeringintobarberton.com) on the western limb of the Onverwacht Anticline. These samples were from the tumulus, a thick, differentiated, entirely serpentinized komatiite flow described by Dann (2001). Three of these latter ten samples are classified as hyaloclastite, one as olivine orthocumulate, one as olivine adcumulate, one as harrisite, two as spinifex textured komatiite, one as pyroxenite, and one as gabbro (Arndt et al., unpublished results).

One additional olivine-cumulate komatiite was collected from the Weltevreden Formation ca. 5 km SW of Barberton (3.5 Ga). The Weltevreden Formation is a lithostratigraphic unit equivalent to the upper part of the Mendon Formation (Fig. 1; Lowe and Byerly, 1999). Its stratigraphic position is younger than the other komatiite and tholeiite samples.

All komatiite and tholeiite samples were collected to reflect the juvenile and unfractionated sulfur source of the Paleoarchean mantle.

3.2. Barite

Twenty-four barite samples were derived from the Mapepe Formation, Fig Tree Group, outcropping in the Barite Syncline in the central part of the Barberton Greenstone Belt (25°53′38″S, 31°4′8″E) (Fig. 1). Beds of detrital barite and barite blades of white or green color and with blades up to 10 cm long are hosted by silicified clastic sedimentary rocks of the Mapepe Formation (Roerdink et al., 2012). The barite is believed to have formed under shallow-water conditions (Reimer, 1980; Lowe and Byerly, 1999). Fourteen of the samples studied here are a subset of Roerdink et al. (2012) and stem from drill core (FT-155.5 to FT-188.2) and from surface outcrops (08-BV and 10-BV) with further stratigraphic and lithological details described in Roerdink et al. (2012). Ten additional samples are from outcrops in Barite Valley from the Mapepe Formation, Fig Tree Group, dated at 3.26-2-3.23 Ga (Heinrichs and Reimer, 1977). Samples were collected at the Conglomerate Quarry Site, to the immediate east of the Barite Syncline. At this site, the barite occurs in different textures: medium-grained, massively-textured and very coarse bladed barite (Gutzmer et al., 2006, with further stratigraphic and lithological details).

The barite is considered to have archived the sulfur isotopic composition of Paleoarchean seawater.

3.3. Black shale

Eleven black shale samples were collected from drill cores at Barbrook Gold Mine reflecting the stratigraphic equivalent of the Mapepe Formation, Fig Tree Group (Fig. 1), but belonging to the northern facies of the Barberton Greenstone Belt (formerly referred to as the Swartkoppie Fm. and the Sheba Fm.). The black shale is characterized by finely disseminated pyrite. Obvious signs of sulfide mineralization, such as massive sulfide bands or larger sulfide aggregates, are absent from these samples, and these black shale samples are considered as an archive reflecting sedimentary and possibly microbial sulfur cycling in the Paleoarchean marine realm.

3.4. Massive and disseminated sulfides

Samples exhibiting massive and disseminated sulfide mineralization stem from the volcano-sedimentary succession in the Barberton Greenstone Belt, notably the Bien Venue (S25°37′28″/E031°21′43″) and M'hlati (S23°51′51″/E030°46′33″) prospects. Six samples belong to the M'hlati ferruginous chert. They are stratigraphically situated in the upper part of the Fig Tree Group (Fig. 1). The M'hlati chert and sulfide precipitates belong to the northern facies within the Barberton Greenstone Belt. The wall rocks represent a very siliceous and ferruginous horizon within the Sheba Formation. Structural and sedimentological examination confirmed that the horizon is associated with the core of a northward-verging, doubly plunging, boat-shaped syncline in Fig Tree Group sediments (Vearncombe, 1986; Stanistreet et al., 1986; in: Ward, 1999). Sulfide mineralization is hosted by distal turbidite and the horizon comprises a silicified banded chert-siltstone-sandstone-mudstone unit. The wall rock is composed

of quartz, chlorite, graphite, carbonates, biotite and zoisite. The mineralized horizon is partly banded and consists mainly of pyrite, hematite, magnetite, quartz, and graphite. Chalcopyrite, pyrrhotite and sphalerite as well as chlorite, biotite, and carbonates are subordinate. Pentlandite, galena, covellite and chalcocite occur as trace components where pyrite dominates in more massive aggregates.

A further nine samples were collected from the Bien Venue prospect (Fig. 1). The Bien Venue Formation, Fig Tree Group, is associated with felsic volcanism and it is characterized by lower greenschist facies metamorphism (Kohler and Anhaeusser, 2002). The Bien Venue Formation was first assigned by Kohler and Anhaeusser (2002) and Kohler (2003) to a new lithostratigraphic unit, forming the uppermost sequence of the Fig Tree Group in the northeastern domain of the Barberton greenstone belt. Consequently, the Bien Venue assemblage overlies the Belvue Road Formation. Conventional U–Pb isotopic studies carried out by Kohler et al. (1993) and Pb–Pb age determinations reported by Kröner (1991) yield an age of 3256 ± 1 Ma and 3259 ± 5 Ma, respectively. The Bien Venue Formation is mainly composed of mica schists and minor talc schists, serpentinites, phyllite-slates, cherts and cherty dolomites. Thereby, quartz-muscovite schists, derived from silicic volcanics, represent by far the most abundant lithology (Kohler, 2003). The schists consist of quartz + muscovite ± andalusite ± pyrophyllite ± chloritoid ± chlorite. Massive sulfide ores at Bien Venue are mainly composed of sphalerite, pyrite, quartz and carbonate minerals. The ore is typically banded, in distal parts disseminated, and contain traces of chalcopyrite, galena, pyrrhotite, cassiterite, several fahlore species (tennantite–tetrahedrite series) and complex Ag–Sn–Sb sulfosalts.

The Bien Venue succession shows a dense intergrowth of barite and pyrite-sphalerite, similar to modern black smoker-type mineralization.

Samples from M'hlati and Bien Venue were collected in order to test for evidence of hydrothermal sulfur cycling in the Paleoarchean oceanic environment.

4. Analytical methods

Bulk rock analyses were performed for all samples, except for barite samples, for which powder was obtained by microdrilling of individual barite blades.

For the powdered bulk rock samples, total sulfur (TS) contents were measured via IR spectroscopy of SO_2 in a CS-MAT 5500, following combustion of the sample powder in an oxygen stream at 1350 °C. Precision and accuracy were determined by replicate measurements of a reference coal sample (NIST) with 1.17 ± 0.03 wt.% total sulfur.

For sulfur isotope analyses, sulfide sulfur was liberated through a wet chemical extraction procedure following Canfield et al. (1986) and Rice et al. (1993). No acid-volatile sulfide (AVS) could be liberated with HCl (25%) as hydrogen sulfide. Chromium-reducible sulfur (CRS – representing solely pyrite as no elemental sulfur was observed) was extracted with chromous (II) chloride solution (1 M $CrCl_2$) with a hot distillation and the resulting hydrogen sulfide was precipitated as zinc sulfide. Zinc sulfide was subsequently converted into silver sulfide (Ag_2S) with 0.1 M silver nitrate ($AgNO_3$) solution.

Barite was reduced to hydrogen sulfide with Thode reduction solution, composed of HI + H_3PO_2 + HCl (Thode et al., 1961). Liberated H_2S was again trapped as zinc sulfide and then converted to Ag_2S.

All silver sulfide precipitates were subjected to traditional sulfur isotopes measurements ($\delta^{34}S$), and multiple sulfur isotope (^{32}S, ^{33}S, ^{34}S, and ^{36}S) measurements were performed for a subset of samples. $\delta^{34}S$ values resulting from both analytical approaches agree within analytical precision.

Traditional sulfur isotopes were measured using a ThermoFinnigan Delta Plus mass spectrometer connected to an elemental analyser (EA-IRMS). Results are expressed as delta values relative to the Vienna Canyon Diablo Troilite (V-CDT):

$$\delta^{34}S(‰,\ \text{V-CDT}) = \left[\left(\frac{(^{34}S/^{32}S)_{sample}}{(^{34}S/^{32}S)_{standard}}\right) - 1\right] \times 1000 \quad (1.1)$$

following Hulston and Thode (1965). The analytical precision as determined through replicate analyses of samples and reference materials was generally better than ±0.3‰ for $\delta^{34}S$. Accuracy of the results was monitored through the analyses of international reference materials (IAEA S1, S2, and S3).

Multiple sulfur isotopes measurements were performed using a ThermoFinnigan MAT 253 following the fluorination of silver sulfide precipitates (cf. Ono et al., 2006). Results were calculated from $\delta^{33}S$, $\delta^{34}S$, and $\delta^{36}S$ and expressed as $\Delta^{33}S$ and $\Delta^{36}S$ values:

$$\Delta^{33}S(‰) = \delta^{33}S - 1000 \times \left[\left(1 + \frac{\delta^{34}S}{1000}\right)^{0.515} - 1\right] \quad (1.2)$$

$$\Delta^{36}S(‰) = \delta^{36}S - 1000 \times \left[\left(1 + \frac{\delta^{34}S}{1000}\right)^{1.90} - 1\right] \quad (1.3)$$

following Farquhar et al. (2000). The analytical precision was ±0.01‰ for $\Delta^{33}S$ and ±0.1‰ for $\Delta^{36}S$. Accuracy of the multiple sulfur isotope measurements was determined by replicate analyses of the international reference material IAEA-S1 ($\delta^{34}S = -0.30‰$). Some of the multiple sulfur isotope measurements were performed at the University of Maryland. For these, the analytical precision on $\Delta^{36}S$ is ±0.3‰.

Finally, the oxygen isotopic composition of barite was measured using a high-temperature pyrolysis unit (ThermoFinnigan TC/EA) coupled to a ThermoQuest Delta Plus XL. Results are reported in the usual $\delta^{18}O$ notation relative to the Vienna Standard Mean Ocean Water (V-SMOW). Measurements are calibrated against international standards (NBS 127, IAEA SO-5, and IAEA SO-6). The analytical precision was ±0.19‰ for $\delta^{18}O$.

5. Results

Analytical results for the four different sample sets are presented in this section and listed in Tables 1 and 2. Komatiites and tholeiites are the oldest samples and they were derived from the Onverwacht Group, specifically the Komati Formation (with a single sample from the Weltevreden Formation). All other samples are from the Fig Tree Group, more specifically from the Mapepe Formation or its stratigraphic equivalent from the northern part of the Barberton Greenstone Belt. Despite the age difference, we still consider the komatiites and tholeiites and their multiple sulfur isotopic composition as being representative for Paleoarchean oceanic crustal rocks when compared to the slightly younger sedimentary rocks from the Fig Tree Group.

5.1. Komatiite and tholeiite

Ten rock samples from the BARB1 drill core show low total sulfur abundances of 0.01–0.08 wt.% (avg. 0.03 wt.%; $n = 10$). Multiple sulfur isotopes were measured for eight out of ten BARB1 core samples and six additional outcrop samples. Samples are characterized by $\delta^{34}S$ values between −0.7 and +5.2‰ (avg. +1.5‰; $n = 14$), negative $\Delta^{33}S$ values between −0.50 and −0.09‰ (avg. −0.27‰; $n = 14$), and positive $\Delta^{36}S$

Table 1
Sample names, formation, total sulfur and the multiple sulfur isotope values for the samples in this study.

Samples	Unit	TS (wt.%)	$\delta^{34}S$ (‰, V-CDT)	σ	$\delta^{34}S$ (‰, V-CDT)	σ	$\Delta^{33}S$ (‰, V-CDT)	σ	$\Delta^{36}S$ (‰, V-CDT)	σ
Barite										
08-BV-01-1	Mapepe Fm.		3.56	0.00						
08-BV-01-2	Mapepe Fm.		3.50	0.01						
08-BV-01-3	Mapepe Fm.		3.55	0.09	3.64	0.01	−0.77	0.02	0.18	0.09
08-BV-01-4	Mapepe Fm.		3.57	0.01						
08-BV-05-1	Mapepe Fm.		3.75	0.05	3.93	0.00	−0.71	0.01	0.94	0.14
08-BV-05-2	Mapepe Fm.		3.40	0.06						
08-BV-05-3	Mapepe Fm.		3.40	0.04						
08-BV-05-4	Mapepe Fm.		3.81	0.02	3.92	0.01	−0.73	0.02	0.98	0.10
08-BV-07-4	Mapepe Fm.		5.84	0.17	6.25	0.01	−0.51	0.01	0.98	0.11
08-BV-07-5	Mapepe Fm.		5.96	0.10						
08-BV-07-6	Mapepe Fm.		5.11	0.04	5.43	0.01	−0.36	0.01	0.97	0.11
08-BV-11-1	Mapepe Fm.		3.09	0.23	3.33	0.01	−0.42	0.01	0.91	0.06
08-BV-11-2	Mapepe Fm.		3.58	0.03						
08-BV-11-3	Mapepe Fm.		3.38	0.14						
08-BV-11-4	Mapepe Fm.		3.73	0.32						
08-BV-12-1	Mapepe Fm.		3.94	0.04	4.01	0.01	−0.47	0.00	1.07	0.02
08-BV-12-2	Mapepe Fm.		4.06	0.41						
08-BV-12-3	Mapepe Fm.		3.88	0.32						
08-BV-12-4	Mapepe Fm.		2.89	0.20	3.10	0.01	−0.34	0.02	0.92	0.11
08-BV-13-1	Mapepe Fm.		3.26	0.00						
08-BV-13-2	Mapepe Fm.		3.90	0.32	4.01	0.01	−0.45	0.01	0.61	0.14
08-BV-13-3	Mapepe Fm.		3.74	0.09	4.07	0.01	−0.44	0.02	0.63	0.05
08-BV-13-4	Mapepe Fm.		3.64	0.11						
10-BV-01-1	Mapepe Fm.		3.96	0.25	3.94	0.01	−0.69	0.01	1.19	0.10
10-BV-01-2	Mapepe Fm.		3.92	0.01	3.98	0.01	−0.71	0.01	1.27	0.06
10-BV-02-1	Mapepe Fm.		3.43	0.02	3.54	0.01	−0.57	0.00	0.97	0.06
10-BV-02-2	Mapepe Fm.		3.61	0.06	3.63	0.01	−0.58	0.01	1.14	0.09
10-BV-02-3	Mapepe Fm.		3.35							
BV-09-1-1	Mapepe Fm.		3.45	0.03	3.55	0.01	−0.52	0.01	0.92	0.09
BV-09-1-2	Mapepe Fm.		3.48	0.08						
BV-09-1-3	Mapepe Fm.		3.45	0.10						
BV-09-3	Mapepe Fm.		3.67	0.08	3.81	0.02	−0.53	0.02	0.74	0.12
155.5-1	Mapepe Fm.		3.37		3.54	0.01	−0.47	0.01	1.10	0.11
155.5-2	Mapepe Fm.		3.37	0.13						
188.2-1	Mapepe Fm.		5.77	0.01	5.78	0.01	−0.45	0.01	0.96	0.09
188.2-2	Mapepe Fm.		6.88	0.31						
188.2-3	Mapepe Fm.		7.67	0.21	8.06	0.01	−0.41	0.02	1.05	0.11
FT-173-1	Mapepe Fm.		3.87	0.00						
FT-173-2	Mapepe Fm.		3.56	0.04	3.96	0.01	−0.63	0.01	1.33	0.02
FT-179-1	Mapepe Fm.		3.56	0.04	3.82	0.01	−0.49	0.02	0.72	0.06
BAR0704-6A	Mapepe Fm.				3.65		−0.64		0.65	
BAR0704-4B-a	Mapepe Fm.				3.54		−0.58		0.50	
BAR0704-3 (2b)	Mapepe Fm.				3.45		−0.66		0.54	
BAR0704-2 (2a)	Mapepe Fm.				3.34		−0.51		0.51	
BAR0704-6-a	Mapepe Fm.				3.38		−0.64		0.57	
BAR0704-4B-b	Mapepe Fm.				3.46		−0.65		0.54	
BAR0704-5	Mapepe Fm.				3.49		−0.58		0.61	
BAR0704-6-c	Mapepe Fm.				3.71		−0.57		0.67	
BAR0704-6B	Mapepe Fm.				3.49		−0.51		0.57	
BAR0704-6-b	Mapepe Fm.				3.42		−0.57		0.55	
Massive and disseminated sulfide ores										
MH4-6	Lower part Fig Tree Group	3.17	−0.80	0.09	−0.39	0.01	3.02	0.00	-1.35	0.05
MH4-7	Lower part Fig Tree Group	2.81	−0.30	0.21	−0.44	0.01	3.12	0.01	-1.61	0.10
MH4-9	Lower part Fig Tree Group	8.13	−0.40	0.02	−0.46	0.01	3.15	0.02	-1.56	0.07
MH4-10	Lower part Fig Tree Group	30.49	−0.10	0.03	−0.09	0.01	3.17	0.02	-1.84	0.14
MH4-12	Lower part Fig Tree Group	1.78	-1.40	0.07	-1.18	0.00	2.66	0.01	-1.16	0.05
MH4-13	Lower part Fig Tree Group	2.00	–	–						
SA-0990	Mapepe Fm.	17.21	1.80	0.07	1.80	0.01	−0.17	0.02	0.79	0.07
SA-0991	Mapepe Fm.	19.45	3.40	0.01	3.48	0.01	−0.16	0.01	1.28	0.05
SA-0614-1	Mapepe Fm.	34.22	1.60	0.28	1.57	0.00	−0.13	0.01	0.65	0.05
SA-0615-4	Mapepe Fm.	30.24	1.60	0.02	1.70	0.01	−0.16	0.02	0.62	0.11
SA-0615-5	Mapepe Fm.	34.86	1.90	0.02	1.89	0.01	−0.15	0.01	0.96	0.09
SA-0615-5-A	Mapepe Fm.	39.64	1.60	0.02	1.74	0.00	−0.17	0.01	0.64	0.64
SA-0615-5-B	Mapepe Fm.	37.65	0.50	0.02	0.66	0.01	−0.13	0.01	1.20	0.04
SA-0615-6	Mapepe Fm.	34.20	1.40	0.04	1.65	0.01	−0.15	0.02	0.66	0.06
SA-0615-7	Mapepe Fm.	21.89	2.70	0.29	2.60	0.01	−0.17	0.01	0.91	0.10
Komatiites and tholeiites										
Barb1 NA/1	Komati Fm.	0.04			1.53	0.00	−0.33	0.02	0.62	0.17
Barb1 NA/2	Komati Fm.	0.08			2.51	0.01	−0.37	0.01	0.85	0.19
Barb1 NA/3	Komati Fm.	0.06			1.72	0.01	−0.28	0.01	0.63	0.08
Barb1 NA/4	Komati Fm.	0.01			2.24	0.01	−0.34	0.02	0.94	0.15

Table 1 (*Continued*)

Samples	Unit	TS (wt.%)	$\delta^{34}S$ (‰, V-CDT)	σ	$\delta^{34}S$ (‰, V-CDT)	σ	$\Delta^{33}S$ (‰, V-CDT)	σ	$\Delta^{36}S$ (‰, V-CDT)	σ
Barb1 NA/5	Komati Fm.	0.01			–	–	–	–	–	–
Barb1 NA/6	Komati Fm.	0.01			0.14	0.01	−0.29	0.01	0.50	0.10
Barb1 NA/7	Komati Fm.	0.01			–	–	–	–	–	–
Barb1 NA/8	Komati Fm.	0.02			4.33	0.01	−0.43	0.02	0.77	0.20
Barb1 NA/9	Komati Fm.	0.03			1.28	0.01	−0.21	0.03	0.64	0.10
Barb1 NA/10	Komati Fm.	0.02			2.23	0.01	−0.30	0.01	0.71	0.09
Za 27	Komatiite lens Weltevreded Fm.				5.17		−0.50		1.90	
Za 29C	Tholeiite, Komati Fm.				0.06		−0.12		0.79	
Za 28B	Komati Fm.				−0.52		−0.18		0.68	
Za 28A	Komati Fm.				0.35		−0.09		0.83	
Za 29A	Tholeiite, Komati Fm.				−0.71		−0.11		1.55	
Za 29B	Tholeiite, Komati Fm.				0.12		−0.20		1.07	
Black shale										
BB 10-29-1	Sheba Fm.	0.09			1.26		0.59		−0.76	
BB 10-29-1	Sheba Fm.	0.07			1.26		1.08		-1.08	
BZ8-30-1	Swartkoppie Fm.	0.22			0.20		2.43		-2.13	
BZ8-30-1	Swartkoppie Fm.	0.20			0.17					
BZ8-30-1	Swartkoppie Fm.	0.94			0.00		2.45		-1.74	
BZ8-30-1	Swartkoppie Fm.	0.87			0.37		2.34		-1.50	
BZ8-30-1	Swartkoppie Fm.	0.55			1.05					
BZ8-30-1	Swartkoppie Fm.	1.56			0.64		2.44		-2.25	
BZ8-30-1	Swartkoppie Fm.	0.43			0.80		2.44		-2.10	
BZ8-30-1	Swartkoppie Fm.	0.43			1.27		1.55			
BZ8-30-1	Swartkoppie Fm.	0.79			1.11		1.51		-1.55	
IAEA-S1					−0.38	0.01	0.07	0.02	−0.38	0.06
IAEA-S1					−0.38	0.00	0.07	0.01	−0.18	0.06
IAEA-S1					−0.46	0.01	0.08	0.01	−0.24	0.07
IAEA-S1					−0.40	0.01	0.08	0.01	−0.34	0.08
IAEA-S1					−0.39	0.01	0.08	0.02	−0.38	0.15
IAEA-S1					−0.41	0.01	0.06	0.02	−0.30	0.25

values between +0.50 and +1.90‰ (avg. +0.89‰; $n = 14$). In general, no difference in sulfur isotopic composition is discernible between drill core and outcrop samples. In addition, however, samples also exhibit a strong negative correlation between $\delta^{34}S$ and $\Delta^{33}S$ ($R^2 = 0.8$) (Fig. 2). Sample Za-27 from the Weltevreden Formation displays the highest $\delta^{34}S$ and the lowest $\Delta^{33}S$ value (this sample shows signs of intense serpentinization).

5.2. Barite

Barite from the Mapepe Formation collected at Barite Valley, Barberton Greenstone Belt, displays a positive sulfur isotopic composition ($\delta^{34}S$), with values ranging between +3.1 and +8.1‰ (avg.

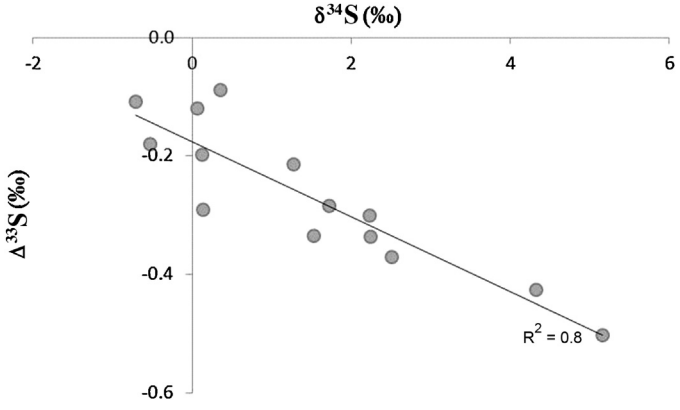

Fig. 2. Sulfur isotope results for komatiites and tholeiites from the Barberton Greenstone Belt. A strong negative correlation is discernible ($R^2 = 0.8$). Samples are enriched in ^{34}S and do not display an unfractionated mantle sulfur isotopic composition. Instead, values reflect the incorporation of a mass-independently fractionated sulfur pool, possibly reflecting interaction with ambient seawater sulfate.

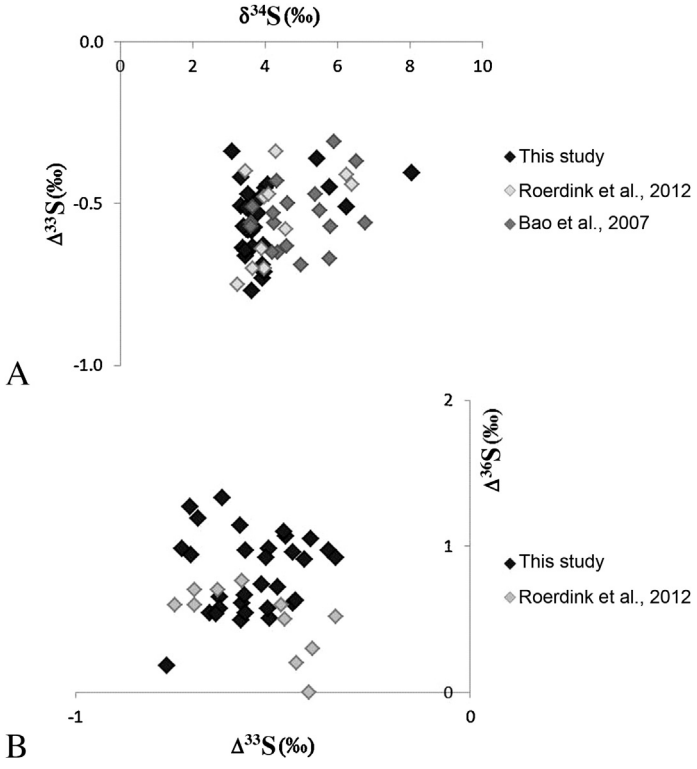

Fig. 3. (A) Plot of $\delta^{34}S$ vs. $\Delta^{33}S$ for barite deposits from the Mapepe Formation, Barberton Greenstone Belt. Our samples confirm previous reports for the barite in the BGB (Bao et al., 2007; Roerdink et al., 2012). Values reported here reflect the oceanic sulfate composition. The sulfur isotopic composition is characterized by non-zero $\delta^{34}S$ and $\Delta^{33}S$ values, thus representing a photolytic origin that was modified via bacterial sulfate reduction. (B) Plot of $\Delta^{33}S$ vs. $\Delta^{36}S$ for barite deposits from the Mapepe Formation, Barberton Greenstone Belt.

Table 2
Sample names, formation and oxygen isotope values for Barite Valley samples.

Samples	Unit	$\delta^{18}O$	σ
08-BV-01-1	Mapepe Fm.	8.99	0.42
08-BV-01-2	Mapepe Fm.	9.57	0.19
08-BV-01-3	Mapepe Fm.	10.24	0.18
08-BV-01-4	Mapepe Fm.	8.98	0.03
08-BV-05-1	Mapepe Fm.	9.83	0.23
08-BV-05-2	Mapepe Fm.	9.68	0.19
08-BV-05-3	Mapepe Fm.	10.89	0.25
08-BV-05-4	Mapepe Fm.	10.56	0.23
08-BV-07-5	Mapepe Fm.	12.43	0.40
08-BV-07-6	Mapepe Fm.	12.96	0.37
08-BV-11-1	Mapepe Fm.	9.36	0.09
08-BV-11-2	Mapepe Fm.	10.66	0.57
08-BV-11-3	Mapepe Fm.	8.59	0.04
08-BV-11-4	Mapepe Fm.	10.40	0.20
08-BV-12-1	Mapepe Fm.	11.83	0.14
08-BV-12-2	Mapepe Fm.	11.40	0.19
08-BV-12-4	Mapepe Fm.	8.92	0.25
08-BV-13-1	Mapepe Fm.	7.62	0.24
08-BV-13-2	Mapepe Fm.	9.61	0.11
08-BV-13-3	Mapepe Fm.	9.70	0.19
08-BV-13-4	Mapepe Fm.	8.94	0.59
BV-09-2	Mapepe Fm.	9.84	0.49
BV-09-3	Mapepe Fm.	9.52	0.14
10-BV-01-1	Mapepe Fm.	10.07	0.18
10-BV-02-1	Mapepe Fm.	10.25	0.17
10-BV-02-2	Mapepe Fm.	10.63	0.07
10-BV-02-3	Mapepe Fm.	9.39	0.30
155.5-1	Mapepe Fm.	8.02	0.33
155.5-2	Mapepe Fm.	9.05	0.37
188.2-1	Mapepe Fm.	11.05	0.07
188.2-2	Mapepe Fm.	11.66	0.21
188.2-3	Mapepe Fm.	12.29	0.06
FT-173-1	Mapepe Fm.	12.19	0.07
FT-173-2	Mapepe Fm.	12.68	0.36
FT-179-1	Mapepe Fm.	11.92	0.13
NBS 127		9.17	0.28
NBS 127		9.50	0.57
NBS 127		9.22	0.26
NBS 127		9.16	0.17
NBS 127		9.44	0.60
NBS 127		9.30	0.10
NBS 127		9.30	0.39
BaSO4 (Lab.)		12.37	0.27
BaSO4 (Lab.)		11.69	0.11
BaSO4 (Lab.)		12.49	0.11
BaSO4 (Lab.)		12.73	0.17

+4.0‰; $n = 41$). A subset of the barite samples was measured for multiple sulfur isotopes. Negative $\Delta^{33}S$ values between −0.77 and −0.34‰ (avg. −0.55‰; $n = 31$) and positive $\Delta^{36}S$ values between +0.18 and +1.33‰ (avg. +0.82‰; $n = 31$) further characterize the barite (Fig. 3A and B).

The oxygen isotopic composition displays a range in $\delta^{18}O$ between +7.6 and +12.9‰ (avg. +10.2‰; $n = 35$). No correlation exists between $\delta^{18}O$ and the minor sulfur isotopes ($\Delta^{33}S$ and $\Delta^{36}S$), and only a very weak correlation is indicated between $\delta^{34}S$ and $\delta^{18}O$ ($R^2 = 0.3$).

5.3. Black shale, non-mineralized

Total sulfur abundances for black shale samples from the stratigraphic equivalent of the Mapepe Formation, northern limb of the Barberton Greenstone Belt, range between 0.07 and 1.56 wt.% and $\delta^{34}S$ values between 0.0 and +1.3‰ (avg. +0.7‰; $n = 12$) (Fig. 4A). The minor sulfur isotopes show positive $\Delta^{33}S$ values, ranging between +0.59 and +2.45‰ (avg. +1.87‰; $n = 10$), and negative $\Delta^{36}S$ values between −2.25 and −0.76‰ (avg. −1.64‰; $n = 8$) (Fig. 4A and B).

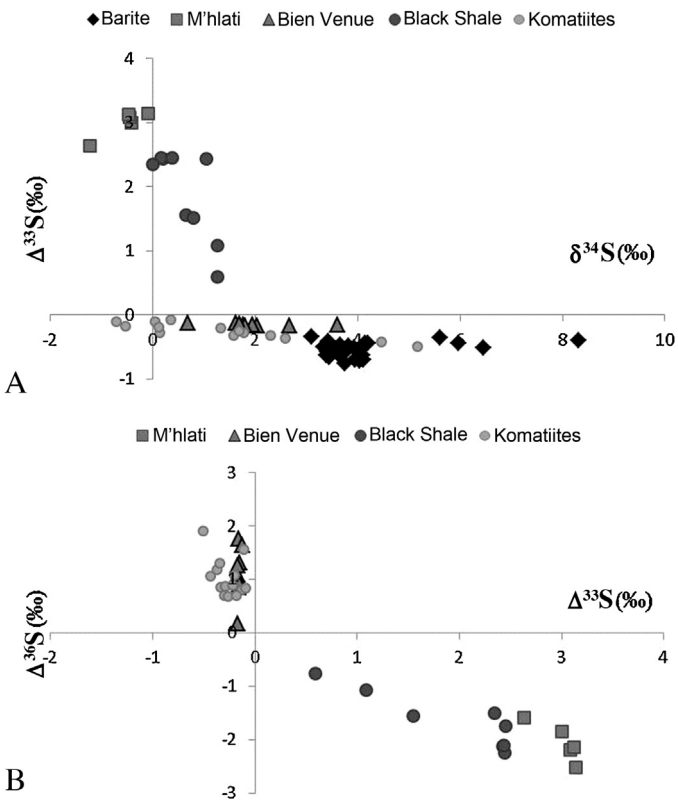

Fig. 4. (A) Plot of $\delta^{34}S$ vs. $\Delta^{33}S$ for sulfides from the M'hlati deposit and the Bien Venue Prospect, as well as for komatiites, barite and black shale sulfides from the Barberton Greenstone Belt. Black shale sulfides show positive $\delta^{34}S$ and positive $\Delta^{33}S$, reflecting an atmospheric source: elemental sulfur. The limited range in $\delta^{34}S$ suggests elemental sulfur reduction. Sulfur isotopes from the Bien Venue deposit overlap with values for komatiites and tholeiites, suggesting a common sulfur source. In contrast, sulfides from M'hlati deposit show negative $\delta^{34}S$ and positive $\Delta^{33}S$, representing incorporation of photolytic elemental sulfur. (B) Plot of $\Delta^{33}S$ vs. $\Delta^{36}S$ for sulfides from the M'hlati deposit and the Bien Venue Prospect, as well as for komatiites, barite and black shale sulfides from the Barberton Greenstone Belt. Samples display the negative correlation between $\Delta^{33}S$ and $\Delta^{36}S$ with a slope of ≈ −1 which is typical for Archean sedimentary sulfur (Farquhar et al., 2000).

5.4. Massive and disseminated sulfide ores

Total sulfur abundances for M'hlati samples range between 1.78 and 30.49 wt.% (avg. 8.06 wt.%; $n = 6$), while Bien Venue sulfides and sulfide-mineralized volcanoclastics display total sulfur abundances between 17.21 and 39.64 wt.% (avg. 29.93 wt.%; $n = 9$).

The Bien Venue sulfides are characterized by positive $\delta^{34}S$ values ranging from +0.7 to +3.5‰ (avg. +1.9‰; $n = 9$), while all M'hlati sulfides display slightly negative $\delta^{34}S$ values between −1.2 and −0.1‰ (avg. −0.5‰; $n = 5$) (Fig. 4A). Thus, samples from M'hlati and samples from Bien Venue show distinctively different ranges in $\delta^{34}S$. Furthermore, both sample sets show very different minor sulfur isotope results. Samples from M'hlati yielded a range of positive $\Delta^{33}S$ values between +2.66 and +3.17‰ (avg. +3.02‰; $n = 5$), while the Bien Venue ores display slightly negative values, varying between −0.17 and −0.12‰ (avg. −0.15‰; $n = 9$) (Fig. 4A and B). In addition, M'hlati samples exhibit $\Delta^{36}S$ values between −1.84 and −1.16‰ (avg. −1.50‰; $n = 5$), while Bien Venue sulfides are characterized by $\Delta^{36}S$ values between +0.62 and +1.28‰ (avg. +0.86‰; $n = 9$).

6. Discussion

Sulfur isotopes represent a strong analytical tool for identifying sulfur sources and for reconstructing processes of sulfur cycling.

Mass-independently fractionated sulfur, recorded as distinct non-zero $\Delta^{33}S$ and $\Delta^{36}S$ values, is thought to identify an atmospheric source of sulfur. In contrast, $\delta^{34}S$ values reflect the mass-dependent sulfur isotopic fractionation during terrestrial inorganic or biological sulfur cycling.

Four different sample sets were studied here, all of Paleoarchean age and originating from the Barberton Greenstone Belt: komatiites and tholeiites from the Komati Formation, Onverwacht Group (including a single sample from the Weltevreden Formation, Mendon Group), and barite, non-mineralized black shale, and volcanic- and sediment-hosted massive and disseminated sulfide ores from the Mapepe Formation (and stratigraphic equivalents), Fig Tree Group. These four lithologically different sample sets were selected in order to constrain sources and processes within the Paleoarchean sulfur cycle: the komatiites and tholeiites are expected to yield a juvenile unfractionated sulfur isotopic composition; the barite is considered reflecting the sulfur isotopic composition of ambient oceanic sulfate; the non-mineralized carbonaceous shale potentially exhibits a sulfur isotopic signature indicative for microbial sulfur cycling, and the massive and disseminated sulfides might reflect signs of hydrothermal sulfur cycling.

6.1. Komatiite and tholeiite

Komatiites and tholeiites from the Komati Formation analyzed here display $\delta^{34}S$ values between −0.7 and 5.2‰ and small but distinct non-zero negative $\Delta^{33}S$ values (between −0.50 and −0.09‰). Thus, in contrast to our expectations, all samples are enriched in ^{34}S with respect to a $\delta^{34}S$ signature of -0.89 ± 0.11‰ for modern MORB and distinctly more negative in $\Delta^{33}S$ than modern MORB ($\Delta^{33}S = 0$‰) as recently defined by Labidi et al. (2012, 2014). Moreover, komatiite and tholeiite samples display a negative correlation between $\delta^{34}S$ and $\Delta^{33}S$ ($R^2 = 0.8$; Fig. 2), and also show a negative correlation between $\Delta^{33}S$ and $\Delta^{36}S$ (Fig. 4B) with a typical Archean slope of ≈−1 (Farquhar et al., 2000).

Clearly, komatiites and tholeiites studied here do not display the expected juvenile sulfur source ("mantle sulfur"). Instead, the distinct non-zero $\Delta^{33}S$ values and the negative correlation between $\Delta^{33}S$ and $\Delta^{36}S$ suggest that these samples reflect the incorporation of a sulfur pool that is characterized by mass independently fractionated sulfur isotopes. Thus, the komatiites and tholeiites exhibit a distinct contribution of sulfur that has experienced photochemistry.

Following our understanding of modern day sulfur cycling in the oceanic realm, the incorporation of a photolytic sulfur component into oceanic crustal rocks could have been achieved either via hydrothermal circulation of seawater through and interaction with oceanic crustal rocks and/or the subduction of oceanic crustal rocks and their sedimentary cover and the subsequent incorporation of volatile phases into the deep mantle.

We propose, as most plausible mechanism, that the multiple sulfur isotopic composition determined for our komatiite and tholeiite samples reflect their (sometimes intense) alteration through interaction with a fluid containing photolytic sulfate (possibly ambient seawater), resulting in a shift away from the expected juvenile sulfur isotopic composition (cf. Labidi et al., 2012, 2014). The seawater alteration of oceanic crustal rocks is a well-known feature from the modern world as well as the ancient oceanic crust and respective changes in $\delta^{34}S$ (e.g., Alt et al., 1989; Alt, 1995; Alt and Shanks, 2003; Peters et al., 2010) and $\Delta^{33}S$ (e.g., Ono et al., 2007; Rouxel et al., 2008; Peters et al., 2010; Oeser et al., 2012) have been reported before.

Support for our interpretation stems from the distinct trajectory defined by the negative correlation between $\delta^{34}S$ and $\Delta^{33}S$ that originates from the expected field of juvenile sulfur (i.e. close to modern MORB; cf. Labidi et al., 2012, 2014) and extends into the field defined by the multiple sulfur isotopic composition of barite from the Mapepe Formation studied here and/or previously published (Bao et al., 2007; Roerdink et al., 2012). On this trajectory, sample Za-27 from the Weltevreden Formation exhibits the most positive $\delta^{34}S$ and the most negative $\Delta^{33}S$ value.

6.2. Barite

The sulfur isotopic composition measured for Paleoarchean barite is thought to represent the sulfur isotopic composition of ambient seawater sulfate. Multiple sulfur isotope data measured here for barite from the Barite Valley display somewhat variable $\delta^{34}S$ values between +3.1 and +8.1‰ and $\Delta^{33}S$ values around an average of −0.55‰ (Fig. 3A), i.e. clearly mass-independently fractionated sulfur isotopes (MIF-S). In general, these results confirm multiple sulfur isotope data previously reported for barite from the Mapepe Formation, Barberton Greenstone Belt (Farquhar et al., 2000; Bao et al., 2007; Roerdink et al., 2012).

The MIF-S signature indicates that the barite sulfate originated as an atmospheric sulfur compound that was subsequently incorporated into Earth's surface environment. Moreover, in the absence of oxidative weathering and much in contrast to the modern world, this atmospheric sulfate represented the dominant source of Paleoarchean oceanic sulfate.

The positive nature and the observed variability in $\delta^{34}S$ suggest further processing of this photolytic sulfate in the marine realm. Respective terrestrial processes would have been associated solely with mass-dependent sulfur isotopic fractionation, thereby preserving the original photolytic signature. Roerdink et al. (2012) attributed the observed $\delta^{34}S$ values of barite from the Mapepe Formation to microbial sulfate reduction, however, on different spatial scales. Considering a $\delta^{34}S$ values of −2‰ and a $\Delta^{33}S$ value of −1‰ for photolytic sulfate (acknowledging the trend reported by Ueno et al., 2008), Roerdink et al. (2012) concluded that the overall positive $\delta^{34}S$ signature for Paleoarchean barite reflects an enrichment in ^{34}S due to global scale microbial sulfate reduction of a limited oceanic sulfate reservoir. The observed variability in $\delta^{34}S$, much in contrast to the very narrow range in $\delta^{34}S$ of modern day oceanic sulfate (e.g., Böttcher et al., 2007), was attributed to further basin-scale alteration of a global background value.

The conclusion that microbial sulfate reduction caused the observed range in $\delta^{34}S$ in the barite is supported by variable and in part distinctly negative $\delta^{34}S$ values for sedimentary pyrite in the Mapepe Formation that are interpreted to reflecting their biogenic nature (Roerdink et al., 2013). The possibility of a microbial origin of Paleoarchean (barite-hosted) microscopic pyrite was previously suggested, e.g., by Shen et al. (2001, 2009) and Philippot et al. (2007), but alternative views have been proposed (e.g., Bao et al., 2008; Philippot et al., 2012; see below).

In summary, we follow Roerdink et al. (2012) in our interpretation and conclude that the Mapepe barite reflects oceanic sulfate. For the sulfate sulfur, multiple sulfur isotope results ($\delta^{34}S$ and $\Delta^{33}S$) indicate a photolytic origin, but the original isotopic composition was subsequently altered via bacterial sulfate reduction.

As for sulfur, the barite oxygen isotopic composition measured here is broadly consistent with results from a previous study by Bao et al. (2007) who reported $\delta^{18}O$ values ranging from +8.9 to 12.9‰ (average of +10.6‰; $n = 49$). A rather weak positive correlation between $\delta^{18}O$ and $\delta^{34}S$ observed here, would be consistent with the proposed activity of sulfate reducing bacteria.

An alternative view for explaining the multiple sulfur isotopic composition of Paleoarchean barite was recently advocated by Philippot et al. (2012), acknowledging an earlier proposition by Bao et al. (2008). These authors concluded that the multiple sulfur isotopic composition of Paleoarchean barite reflects a photolytic sulfate source where the original sulfur isotopic composition might

have been modified by bacterial or abiological sulfate reduction. However, in order to fully explain their reported sulfide sulfur isotope data, Philippot et al. (2012) propose the mixing of photolytic sulfate (subsequently modified by bacterial sulfate reduction) and photolytic elemental sulfur (resulting from a specific MIF-S source reaction), defining a series of different arrays in a $\delta^{34}S$–$\Delta^{33}S$ diagram (their felsic volcanic array, respectively felsic volcanic wedge), mostly with a negative slope.

6.3. Black shale

Pyrite in black shale samples from the Fig Tree Group has been studied to search for sulfur isotopic evidence of microbial sulfur cycling. Three different pathways of microbial sulfur metabolism have been proposed previously for the Paleoarchean: elemental sulfur disproportionation (Philippot et al., 2007; Wacey et al., 2010, 2011a), sulfate reduction (Shen et al., 2001, 2009; Ueno et al., 2008; Wacey et al., 2010, 2011a) and sulfide oxidation (Wacey et al., 2011b).

As mentioned before, microbially driven sulfur cycling is associated solely with mass-dependent sulfur isotopic fractionation and would not obliterate non-zero $\Delta^{33}S$ or $\Delta^{36}S$ values indicative of a photolytic origin of the sulfur. In principle, sedimentary sulfides exhibiting a combination of positive $\delta^{34}S$ and positive $\Delta^{33}S$ values reflect incorporation of an atmospheric sulfur source, notably elemental sulfur, whereas sulfides showing negative $\delta^{34}S$ and negative $\Delta^{33}S$ values indicate that sulfide sulfur resulted from the bacterial fractionation of atmospheric sulfate (e.g., Johnston, 2011, and references therein).

Black shale samples studied here show positive $\delta^{34}S$ values between 0.0 and +1.3‰ and positive $\Delta^{33}S$ values between +0.59 and +2.45‰ (Fig. 4A). Clearly, pyrite sulfur from black shale samples has archived a mass-independent atmospheric source signal. Following previous accounts (e.g., Farquhar et al., 2000; Johnston, 2011), the positive $\Delta^{33}S$ signature of the sedimentary pyrite suggests the incorporation of photolytic elemental sulfur rather than photolytic sulfate, the latter generally carrying a negative $\Delta^{33}S$ value.

In order to form pyrite, the (photolytic) elemental sulfur would have to be reduced which could have happened either via elemental sulfur disproportionation or via elemental sulfur reduction (Thamdrup et al., 1993; Canfield and Raiswell, 1999). Both microbial processes are associated with a fractionation in $\delta^{34}S$ of different magnitude, leaving the $\Delta^{33}S$ and $\Delta^{36}S$ signatures unaltered (Johnston et al., 2005, 2007; Shen et al., 2009). $\delta^{34}S$ values recorded here for the black shale samples are positive and show a low fractionation in ^{34}S (Fig. 4A). This rather limited range in $\delta^{34}S$, and thus a rather limited range in sulfur isotopic fractionation, would be more consistent with elemental sulfur reduction, because this processes is not associated with a high magnitude, mass-dependent sulfur isotopic fractionation (Surkov et al., 2012), compared to the larger fractionation due to elemental sulfur disproportionation (Canfield et al., 1998; Johnston et al., 2005). Our data are in contrast to results from Roerdink et al. (2013) reporting negative $\delta^{34}S$ and $\Delta^{33}S$ values for pyrite in layered and massive pyrite and disseminated pyrite in barite from Mapepe Formation, that suggest the microbial reduction of oceanic sulfate as their ultimate source.

Interestingly, $\delta^{34}S$ and $\Delta^{33}S$ values measured here for the black shale samples are negatively correlated, much in contrast to previous observations of a generally positive correlation between both sulfur isotope signals for Archean and early Paleoproterozoic sedimentary sulfides (for a recent review, see Johnston, 2011). A similar negative correlation was recently proposed by Philippot et al. (2012) to reflect mixing between a sulfide sulfur isotopic composition resulting from a photolytic elemental sulfur source and a sulfide sulfur isotopic composition reflecting mass-dependent bacterial (or abiological) reduction of photolytic sulfate in the ocean.

6.4. Massive and disseminated sulfide ores

Two sets of massive and disseminated sulfide samples from the M'hlati and the Bien Venue prospects show quite different multiple sulfur isotopic compositions. Massive sulfides from Bien Venue display a limited range of positive $\delta^{34}S$ values between +0.7 and +3.5‰, and slightly negative $\Delta^{33}S$ between −0.17 and −0.12‰, overlapping with the range of values defined by the komatiites and tholeiites from this study (Fig. 4A). This suggests in part a common sulfur source. The combined positive $\delta^{34}S$ values and only minor negative displacement in $\Delta^{33}S$ from zero per mil would be consistent with unfractionated juvenile magmatic sulfur as the primary sulfur source but a contribution from recycled ambient seawater sulfate cannot be ruled out. Notably, the range in $\delta^{34}S$ is quite comparable to the relationship between modern hydrothermal sulfides and their magmatic host rocks (e.g., Peters et al., 2010, 2011).

Bekker et al. (2009) and Fiorentini et al. (2012) reported negative $\Delta^{33}S$ values for volcanogenic massive sulfide deposits (VMS) associated with hydrothermal circulation from the ~2.71 Ga Agnew and Norseman Wiluna greenstone belts of Western Australia and the time-equivalent Abitibi Greenstone Belt of Canada; Jamieson et al. (2006) reported negative $\Delta^{33}S$ values for the Archean Kidd Creek volcanogenic massive sulfide (~2.71 Ga), Ontario, Canada. Such data reflect the transfer of a mass-independently fractionated (i.e. an atmospheric) sulfur isotope signal, notably photolytic sulfate, to igneous rocks and also to the mantle.

In contrast, massive and disseminated sulfides from M'hlati are characterized by a different multiple sulfur isotopic composition with negative $\delta^{34}S$ values between −1.2 and −0.1‰ and positive $\Delta^{33}S$ values between +2.66 and +3.17‰. Again, these samples clearly exhibit the incorporation of an atmospheric MIF-S signal, notably photolytic elemental sulfur with positive $\Delta^{33}S$ values (Fig. 4A and B). The small mass-dependent fractionation visible in the $\delta^{34}S$ values may be related to elemental sulfur reduction or disproportionation.

Thus, the two different massive and disseminated sulfides are characterized by different sulfur sources and processes of subsequent sulfur cycling. Multiple sulfur isotope data for sulfides from the Bien Venue prospect would be consistent with the hydrothermal cycling of ambient seawater sulfate reflecting its photolytic origin as sulfate. In contrast, sulfides from M'hlati suggest the incorporation of photolytic elemental sulfur.

7. Conclusions

Our multiple sulfur isotopes for lithologically different rocks from the Paleoarchean Barberton Greenstone Belt, South Africa, allow drawing the following conclusions:

1. Komatiites and tholeiites do not show the expected unfractionated sulfur pool of juvenile magmatic sulfur. Instead, non-zero negative $\Delta^{33}S$ values for sulfide sulfur in these rocks clearly indicate the incorporation of mass-independently fractionated, i.e. atmospheric sulfur. Together with variably positive $\delta^{34}S$ values and a negative correlation with $\Delta^{33}S$, these results may best be explained by the alteration of oceanic crustal rocks through interaction with ambient seawater sulfate and incorporation of photolytic sulfate sulfur carrying a respective negative $\Delta^{33}S$ signature.
2. Barite sulfur displays a mass-independent isotopic fractionation signal, as reported previously for Paleoarchean barite. Values reveal a dominant atmospheric sulfate sulfur source, reflecting

the UV induced photochemical dissociation of volcanogenic SO_2. Subsequently, the sulfur isotopic composition of this sulfate was modified via bacterial sulfate reduction (cf. Roerdink et al., 2012).

3. Massive and disseminated sulfides from the Bien Venue prospect resemble results obtained from komatiite and tholeiites samples, suggesting a common sulfur source. Unfractionated juvenile magmatic sulfur appears to be the dominant sulfur source, but a contribution via recycled photolytic seawater sulfate to the sulfide sulfur in these samples cannot be ruled out.
4. Barite and komatiites and tholeiites, display comparable multiple sulfur isotope values, suggesting a common sulfur source. This source is characterized by negative $\Delta^{33}S$ and positive $\Delta^{36}S$ values, representing ambient seawater sulfate. Individual lithologies, however, are characterized by variable $\delta^{34}S$ values suggesting further modification of the photolytic source signature via bacterial sulfate reduction.
5. Massive and disseminated sulfides from Bien Venue suggest unfractionated magmatic sulfur to be the prominent sulfur source, but a contribution from recycled seawater sulfate cannot be ruled out and would be consistent with the submarine origin of this sulfide mineralization.
6. Massive and disseminated sulfides from the M'hlati prospect show a different sulfur isotopic composition with negative $\delta^{34}S$ and positive $\Delta^{33}S$ values. The latter clearly reflect mass-independent sulfur isotopic fractionation, thus indicating the incorporation of an atmospheric signature, notably photolytic elemental sulfur carrying a positive $\Delta^{33}S$ value.
7. Sedimentary pyrite in black shale samples exhibit positive $\delta^{34}S$ and positive $\Delta^{33}S$ values, both defining a negative correlation. The positive $\Delta^{33}S$ signature clearly indicates photolytic elemental sulfur as the principal sulfur source, but a mixing with sulfide sulfur resulting from bacterial reduction of photolytic sulfate cannot be ruled out (cf. Philippot et al., 2012).

Acknowledgements

HS acknowledges financial support from the Deutsche Forschungsgemeinschaft (DFG Str 281/36). JF gratefully acknowledges financial support from the National Science Foundation (NSF EAR1251804). Artur Fugman and Andreas Lutter are gratefully acknowledged for their skillful laboratory work in the Münster Isotope Research Center (MIRC).

References

Alt, J.C., Anderson, T.F., Bonnell, L., 1989. The geochemistry of sulfur in a 1.3 km section of hydrothermally altered oceanic crust, DSDP Hole 504B. Geochim. Cosmochim. Acta 53, 1011–1023.
Alt, J.C., 1995. Sulfur isotopic profile through the oceanic crust: sulfur mobility and seawater-crustal sulfur exchange during hydrothermal alteration. Geology 23, 585–588.
Alt, J.C., Shanks III, W.C., 2003. Serpentinization of abyssal peridotites from the MARK area, Mid-Atlantic Ridge: sulfur geochemistry and reaction modeling. Geochim. Cosmochim. Acta 67, 641–653.
Anbar, A.D., Duan, Y., Lyons, T.W., Arnold, G.L., Kendall, B., Creaser, R.A., Kaufman, Al.J., Gordon, G.W., Scott, C., Garvin, J., Buick, R., 2007. A whiff of oxygen before the great oxidation event? Science 317, 1903–1906.
Bao, H., Rumble III, D., Lowe, D.R., 2007. The five stable isotope compositions of Fig Tree barites: implications on sulfur cycle in ca. 3.2 Ga oceans. Geochim. Cosmochim. Acta 71, 4868–4879.
Bao, H., Sun, T., Kohl, I., Peng, Y., 2008. Comment on Early Archaean microorganisms preferred elemental sulfur, not sulfate. Science 319, 1336.
Bekker, A., Barley, M.E., Fiorentini, M.L., Rouxel, O.J., Rumble, D., Beresford, S.W., 2009. Atmospheric sulfur in Archean Komatiite-hosted nickel deposits. Science 326, 1086–1098.
Blumenberg, M., Krüger, M., Nauhaus, K., Talbot, H.M., Oppermann, B.I., Seifert, R., Pape, T., Michaelis, W., 2006. Biosynthesis of hopanoids by sulfate-reducing bacteria (genus *Desulfovibrio*). Environ. Microbiol. 8 (7), 1220–1227.
Böttcher, M.E., Brumsack, H.J., Dürselen, C.D., 2007. The isotopic composition of modern seawater sulfate: I. Coastal waters with special regard to the North Sea. J. Mar. Syst. 67 (1), 73–82.
Canfield, D.E., Raiswell, R., Westrich, J.T., Reaves, C.M., Berner, R.A., 1986. The use of chromium reduction in the analysis of reduced inorganic sulfur in sediments and shales. Chem. Geol. 54, 149–155.
Canfield, D.E., Thamdrup, B., Fleischer, S., 1998. Isotope fractionation and sulfur metabolism by pure and enrichment cultures of elemental sulfur-disproportionating bacteria. Limnol. Oceanogr. 34, 253–264.
Canfield, D.E., Raiswell, R., 1999. The evolution of the sulfur cycle. Am. J. Sci. 299, 697–723.
Canfield, D.E., 2001. Isotope fractionation by natural populations of sulfate-reducing bacteria. Geochim. Cosmochim. Acta 65, 1117–1124.
Canfield, D.E., 2004. The evolution of the Earth surface sulfur reservoir. Am. J. Sci. 304, 839–861.
Clark, I., Fritz, P., 1997. Environmental Isotopes in Hydrogeology. CRS Press.
Crowe, S.A., Døssing, L.N., Beukes, N.J., Bau, M., Kruger, S.J., Frei, R., Canfield, D.E., 2013. Atmospheric oxygenation three billion years ago. Nature 501, 535–538.
Crowe, S.A., Paris, G., Katsev, S., Jones, C., Kim, S.T., Zerkle, A.L., Nomosatryo, S., Fowle, D.A., Adkins, J.F., Sessions, A.L., Farquhar, J., Canfield, D.E., 2014. Sulfate was a trace constituent of Archean seawater. Science 346, 735–739.
Dann, J.C., 2000. The 3.5 Ga Komati Formation, Barberton Greenstone Belt, South Africa, Part I: new maps and magmatic architecture. S. Afr. J. Geol. 103, 47–68.
Dann, J.C., 2001. Vesicular komatiites, 3.5-Ga Komati Formation, Barberton Greenstone Belt, South Africa: inflation of submarine lavas and origin of spinifex zones. Bull. Volcanol. 63, 462–481.
Farquhar, J., Bao, H., Thiemens, M., 2000. Atmospheric influence of Earth's earliest sulphur cycle. Science 289, 756–758.
Farquhar, J., Wing, B.A., McKeegen, K.D., Harris, J.W., Cartigny, P., Thiemens, M.H., 2002. Mass-independent sulfur of inclusions in diamond and sulfur recycling on early Earth. Science 298, 2369–2372.
Farquhar, J., Zerkle, A.L., Bekker, A., 2010. Geological constraints on the oxygenic photosynthesis. Photosynth. Res. 107, 11–36.
Fiorentini, M., Beresford, S., Barley, M., Duuring, P., Bekker, A., Rosengren, N., Cas, R., Hronsky, J., 2012. District to camp controls on the genesis of the Komatiite-hosted nickel sulfide deposits, Agnew-Wiluma Greenstone Belt, Western Australia: insight from the multiple sulfur isotopes. Econ. Geol. 105, 781–796.
Frei, R., Gaucher, C., Poulton, S.W., Canfield, D.E., 2009. Fluctuations in Precambrian atmospheric oxygenation recorded by chromium isotopes. Nature 461, 250–253.
Garvin, J., Buick, R., Anbar, A.D., Arnold, G.L., Kaufman, A.J., 2009. Isotopic evidence for an aerobic nitrogen cycle in the latest Archean. Science 323, 1045–1048.
Guo, Q., Strauss, H., Kaufam, A.J., Schröder, S., Gutzmer, J., Wing, B., Baker, M.A., Bekker, A., Jin, Q., Kim, S.T., Farquhar, J., 2009. Reconstructing Earth's surface oxidation across the Archean-Proterozoic transition. Geology 37, 399–402.
Gutzmer, J., Banks, D., de Kock, M.O., McClung, C.R., Strauss, H., Mezger, K., 2006. The origin and paleoenvironmental significance of stratabounds barite from the Mesoarchean Fig Tree Group, Barberton Mountainland, South Africa. In: Trans. of the V South American Symp. on Isotope Geology, contrib. 311, pp. 258–262.
Habicht, K.S., Gade, M., Thamdrup, B., Berg, P., Canfield, D.E., 2002. Calibration of sulfate levels in the Archean Ocean. Science 298, 2372–2374.
Heinrichs, T.K., Reimer, T., 1977. A sedimentary barite deposit from the Archean Fig Tree Group of the Barberton Montain Land (South Africa). Econ. Geol. 72, 1426–1441.
Holland, H.D., 2002. Volcanic gases, black smokers, and the Great Oxidation Event. Geochim. Cosmochim. Acta 66, 3811–3826.
Holland, H.D., Turekian, K.K., 2004. In: Schlesinger, W.H. (volume Ed.), Treatise on Geochemistry, vol. 8: Biogeochemistry. Elvesier Pergamon, Amsterdam.
Holland, H.D., 2006. The oxygenation of atmosphere and ocean. Philos. Trans. R. Soc. B 361, 903–915.
Hulston, J.R., Thode, H.G., 1965. Variations in the S33, S34, and S36 contents of meteorites and their relation to chemical and nuclear effects. J. Geophys. Res. 70, 3475–3484.
Jamieson, J.W., Wing, B., Hannington, M.D., Farquhar, J., 2006. Evaluating isotopic equilibrium among sulfide mineral pairs in Archean Ore Deposits: case study from the Kidd Creek VMS Deposit, Ontario, Canada. Econ. Geol. 101, 1055–1061.
Johnston, D.T., Farquhar, J., Wing, B.A., Kaufman, A.J., Canfield, D.E., Habicht, K.S., 2005. Multiple sulfur isotope fractionations in biological system: a case study with sulfate reducers and sulfur disproportionation. Am. J. Sci. 305, 645–660.
Johnston, D.T., Farquhar, J., Canfield, D.E., 2007. Sulfur isotopes insight into microbial sulfate reduction: when microbes meet models. Geochim. Cosmochim. Acta 71, 3929–3947.
Johnston, D., 2011. Multiple sulfur isotopes and the evolution of Earth's surface sulfur cycle. Earth-Sci. Rev. 106, 161–183.
Kampschulte, A., Strauss, H., 2004. The sulfur isotopic evolution of Phanerozoic seawater based on the analysis of structurally substituted sulfate in carbonates. Chem. Geol. 204, 255–286.
Kohler, E.A., Anhaeusser, C.R., Isachsen, C., 1993. The Bien Venue Formation: a proposed new unit in the northeastern sector of the Barberton greenstone belt. In: Abstracts 16th Colloquium African Geology, pp. 186–188.
Kohler, E.A., Anhaeusser, C.R., 2002. Geology and geodynamic setting of Archaean silicic metavolcaniclastic rocks of the Bien Venue Formation, Fig Tree Group, northeast Barberton greenstone belt, South Africa. Precambrian Res. 116, 199–235.
Kohler, E.A., 2003. The geology of the Archaean granitoid-greenstone terrain in the vicinity of Three Sisters. Barberton Greenstone Belt: Geol. Survey S. Afr. Bull. 133, p150.

Kröner, A., 1991. Tectonic evolution in the Archaean and Proterozoic. Tectonophysics 187 (4), 393–410.
Labidi, J., Cartigny, P., Birck, J.L., Assayag, N., Bourrand, J.J., 2012. Determination of multiple sulfur isotopes in glasses: a reappraisal of the MORB δ^{34}S. Chem. Geol. 334, 189–198.
Labidi, J., Cartigny, P., Hamelin, C., Moreira, M., Dosso, L., 2014. Sulfur isotope budget (32S, 33S, 34S and 36S) in Pacific–Antarctic ridge basalts: a record of mantle source heterogeneity and hydrothermal sulfide assimilation. Geochim. Cosmochim. Acta 133, 47–67.
Lasaga, A.C., Otake, T., Watanabe, Y., Ohmoto, H., 2008. Anomalous fractionation of sulfur isotopes during heterogeneous reactions. Earth Planet. Sci. Lett. 268, 225–238.
Lowe, G.R., Byerly, G.R., 1999. Stratigraphy of the west-central part of the Barberton greenstone belt, South Africa. In: Lowe, G.R., Byerly, G.R. (Eds.), Geologic Evolution of the Barberton Greenstone Belt, South Africa. Spec. Pap. Geol. Soc. Amer., 329. , pp. 1–36.
Münker, C., Pfänder, J.A., Weyer, S., Büchl, A., Kleine, T., Mezger, K., 2003. Evolution of planetary cores and the Earth–Moon system from Nb/Ta systematics. Science 301, 84–87.
Oeser, M., Strauss, H., Wolff, P.E., Koepke, J., Peters, M., Garbe-Schönberg, D., Dietrich, M., 2012. A profile of multiple sulfur isotopes through the Oman ophiolite. Chem. Geol. 312–313, 27–46.
Oduro, H., Harms, B., Sintim, H.O., Kaufman, A.J., Cody, G., Farquhar, J., 2011. Evidence of magnetic isotopes effects during thermochemical sulfate reduction. Proc. Natl. Acad. Sci. U.S.A. 108, 17635–17638.
Ohmoto, H., Kakegawa, T., Lowe, D.R., 1993. 3.4-billion-year-old biogenic pyrites from Barberton, South Africa: sulfur isotope evidence. Science 262, 555–557.
Ohmoto, H., Watanabe, Y., Lasaga, A.C., Naraoka, H., Johnson, I., Brainard, J., Chorney, A., 2014. Oxygen, iron, and sulfur geochemical cycles on early Earth: paradigms and contradictions. Geol. Soc. Am. Spec. Pap. 504, 55–95.
Ono, S., Eigenbrode, J.L., Pavlov, A.A., Kharecha, P., Ruble, D., Kasting, J.F., Freeman, K.H., 2003. New insights into Archean sulfur cycle from mass-independent sulfur isotope records from the Hamersley Basin, Australia. Earth Planet. Sci. Lett. 213, 15–30.
Ono, S., Beukes, N.J., Rumble, D., Fogel, M.L., 2006. Early evolution of atmospheric oxygen from multiple-sulfur and carbon isotope records of the 2.9 Ga Mozaan Group of the Pongola Supergroup, Southern Africa. S. Afr. J. Geol. 109, 97–108.
Ono, S., Shanks III, W.C., Rouxel, O.J., Rumble, D., 2007. S-33 constraints on the seawater sulfate contribution in modern seafloor hydrothermal vent sulfides. Geochim. Cosmochim. Acta 71, 1170–1182.
Papineau, D., Mojzsis, S.J., Schmitt, A.K., 2007. Multiple sulfur isotopes from Paleoproterozoic Huronian interglacial sediments and the rise of atmospheric oxygen. Earth Planet. Sci. Lett. 255, 188–212.
Patyniak, M., Unpublished results. Geochemical characterisation of komatiites and tholeiites from the Komatii Formation, South Africa (BSc Thesis), University of Cologne.
Pavlov, A.A., Kasting, J.F., 2002. Mass-independent fractionation of sulphur isotopes in Archaean sediments: strong evidence for an anoxic Archaean atmosphere. Astrobiology 2, 27–41.
Peters, M., Strauss, H., Farquhar, J., Ockert, C., Eickmann, B., Jost, C.L., 2010. Sulfur cycling at the Mid-Atlantic Ridge: a multiple sulfur isotope approach. Chem. Geol. 269, 180–196.
Peters, M., Strauss, H., Petersen, S., Kummer, N.A., Thomazo, C., 2011. Hydrothermalism in the Tyrrhenian Sea: inorganic and microbial sulfur cycling as revealed by geochemical and multiple sulfur isotope data. Chem. Geol. 280, 217–231.
Philippot, P., Van Zuilen, M., Lepot, K., Thomazo, C., Farquhar, J., Van Kranendonk, M.J., 2007. Early Archaean microorganisms preferred elemental sulfur, not sulfate. Science 317, 1534–1537.
Philippot, P., van Zuilen, M., Rollio-Bard, C., 2012. Variation in atmospheric sulphur chemistry on early Earth linked to volcanic activity. Nat. Geosci. 5, 668–674.
Pufahl, P., Hiatt, E., 2012. Oxygenation of the Earth's atmosphere-ocean system: a review of physical and chemical sedimentologic responses. Mar. Petrol. Geol. 32, 1–20.
Reimer, T.O., 1980. Archean sedimentary baryte deposits of the Swaziland Supergroup (Barberton Mountain Land, South Africa). Precambrian Res. 12, 393–410.
Reinhard, C.T., Raiswell, R., Scott, C., Anbar, A.D., Lyons, T.W., 2009. A late Archean sulfidic sea stimulated by early oxidative weathering of the continents. Science 326, 713–716.
Reuschel, M., Strauss, H., Lepland, A., Melezhik, V.A., Cartigny, P., Kaufmann, A.J., 2009. Multiple sulfur isotope measurements from the 2.4 Ga old Seidorechka Formation. In: Goldschmidt Conference Abstracts 2009.
Rice, C.A., Tuttle, M.L., Reynolds, R.L., 1993. The analysis of forms of sulfur in ancient sediments and sedimentary rocks: comments and cautions. Chem. Geol. 107, 83–95.
Robin-Popieul, C.C.M., Arndt, N.T., Chauvel, C., Byerly, G.R., Sobolev, A.V., Wilson, A., 2012. A new model for Barberton Komatiites: deep critical melting with high melt retention. J. Petrol. 53 (11), 2191–2229.
Roerdink, D.L., Mason, P.R.D., Farquhar, J., Reimer, T., 2012. Multiple sulfur isotopes in Paleoarchean barites identify an important role for microbial sulfate reduction in the early marine environment. Earth Planet. Sci. Lett. 331–332, 177–186.
Roerdink, D.L., Mason, P.R.D., Whitehouse, M.J., Reimer, T., 2013. High-resolution quadruple sulfur isotope analyses of 3.2 Ga pyrite from the Barberton Greenstone Belt in South Africa reveal distinct environmental controls on sulfide isotopic arrays. Geochim. Cosmochim. Acta 117, 203–215.
Rollinson, H.R., 2007. Early Earth Systems: A Geochemical Approach. John Wiley & Sons.
Rouxel, O., Shank III, W.C., Bach, W., Edwards, K.J., 2008. Integrated Fe- and S-isotope study of seafloor hydrothermal vents at East Pacific Rise 9–10°N. Chem. Geol. 252, 214–227.
Seal, R.R., 2006. Sulfur isotope geochemistry of sulfide minerals. Rev. Mineral. Geochem. 61, 633–677.
Shen, Y., Buick, R., Canfield, D.E., 2001. Isotopic evidence for microbial sulphate reduction in the early Archaean era. Nature 410, 77–81.
Shen, Y., Buick, R., 2004. The antiquity of microbial sulfate reduction. Earth-Sci. Rev. 64, 243–272.
Shen, Y., Farquhar, J., Masterson, A., Kaufman, A.J., Buick, R., 2009. Evaluating the role of microbial sulfate reduction in the early Archean using quadruple isotope systematics. Earth Planet. Sci. Lett. 279, 383–391.
Stanistreet, I.G., McCarthy, T.S., Charlesworth, E.G., Myers, R.E., Armstrong, R.A., 1986. Pre-Transvaal wrench tectonics along the northern margin of the Witwatersrand Basin, South Africa. Tectonophysics 131 (1), 53–74.
Strauss, H., 1997. The isotopic composition of sedimentary sulfur through time. Palaeogeogr. Palaeoclimatol. Palaeoecol. 132, 97–118.
Strauss, H., 2003. Sulphur isotopes and the Early Archean sulphur cycle. Precambrian Res. 126, 349–361.
Surkov, A.V., Böttcher, M.E., Kuever, J., 2012. Sulphur isotope fractionation during the reduction of elemental sulphur and thiosulphate by *Dethiosulfovibrio* spp. Isotopes Environ. Health Stud. 48 (1).
Thamdrup, B., Finster, K., Hansen, J.W., Bak, F., 1993. Bacterial disproportionation of elemental sulfur coupled to chemical reduction of iron and manganese. Appl. Environ. Microbiol. 59, 101–108.
Thode, H.G., Monster, J., Dunford, H.B., 1961. Sulphur isotope geochemistry. Geochim. Cosmochim. Acta 25, 159–174.
Ueno, Y., Ono, S., Rumble, D., Maruyama, S., 2008. Quadruple sulfur isotope analysis of ca. 3.5 Ga Dresser Formation: new evidence for microbial sulfate reduction in the early Archean. Geochim. Cosmochim. Acta 72, 5675–5691.
Vearncombe, J.R., 1986. Structure of veins in a gold–pyrite deposit in banded iron formation, Amalia greenstone belt, South Africa. Geol. Magazine 123 (06), 601–609.
Viljoen, M.J., Viljoen, R.P., 1969. The geological and geochemical significance of the upper formations of the Onverwacht Group. Spec. Publ. Geol. Soc. S. Afr. 2, 113–151.
Visser, D.J.L. (Comp), 1956. The geology of the Barberton area. Spec. Publ Geol. Szrv. S. Afr., 15, 253.
Wacey, D., McLoughlin, N., Whitehouse, M.J., Kilburn, M.R., 2010. Two coexisting sulfur metabolisms in a ca. 3400 Ma sandstone. Geology 38, 1115–1118.
Wacey, D., Kilburn, M.R., Saunders, M., Cliff, J., Brasier, M.D., 2011a. Microfossils of sulphur-metabolizing cells in 3.4-billion-year-old rocks of Western Australia. Nat. Geosci. 4, 698–702.
Wacey, D., Saunders, M., Brasier, M.D., Kilburn, M.R., 2011b. Earliest microbially mediated pyrite oxidation in ~3.4 billion-year-old sediments. Earth Planet. Sci. Lett. 301, 393–402.
Ward, J.H.W., 1999. The metallogeny of the Barberton greenstone belt – South Africa and Swaziland. Council for Geoscience. Gel Survey S. Afr. Mem. 86, 1–108.
Watanabe, Y., Farquhar, J., Ohmoto, H., 2009. Anomalous fractionations of sulfur isotopes during thermochemical sulfate reduction. Science 324, 370–373.
Wu, N., Farquhar, J., 2013. Metabolic rates and sulfur cycling in the geological record. Proc. Natl. Acad. Sci. U.S.A. 110, 11217–11218.